Topological Analysis of the Reaction of Mn^+ (^7S,^5S) with H_2O, NH_3, and CH_4 Molecules

Maria del Carmen Michelini, Emilia Sicilia, and Nino Russo*,†

Dipartimento di Chimica and Centro di Calcolo ad Alte Prestazioni per Elaborazioni Parallele e Distribuite-Centro d'Eccellenza MURST, Università della Calabria, I-87030 Arcavacata di Rende, Italy

Mohamnad Esmail Alikhani

Laboratoire de Dynamique, Interactions et Réactivité (UMR 7075), Université P. et M. Curie, Boite 49, batiment F74, 4 Place Jussieu, 75252-Paris Cedex 05, France

Bernard Silvi

Laboratoire de Chimie Théorique (UMR 7616), Université P. et M. Curie, Boite 137, Tour 22−23, 4 Place Jussieu, 75252-Paris Cedex 05, France

Received: October 30, 2002; In Final Form: April 16, 2003

The potential energy surfaces (PES) for the interaction of Mn^+ (^7S, ^5S) with H_2O, NH_3, and CH_4 have been studied within the framework provided by the electron localization function (ELF) analysis. This has been achieved by analyzing density functional theory calculations (B3LYP approach) using the bonding evolution theory. The main characteristic of the studied reactions is the involvement of more than a single spin surface in the reaction pathways, which means that a spin crossover occurs along the reaction coordinate. This type of reactions are usually classified in terms of the two-state reactivity (TSR) paradigm. The different domains of structural stability occurring along the reaction path have been identified as well as the bifurcation catastrophes responsible for the changes in the topology of the systems. The analysis provides a chemical description of the reaction mechanism in terms of agostic bond formation and breaking.

1. Introduction

During the last 2 decades, extensive experimental and theoretical work has focused on the investigation of the ability of "naked" transition-metal ions to activate small molecules in gas-phase.[1−37] Such studies provide thermochemical details and some insights on the reaction mechanisms.

The growing interest in these kinds of reactions has been prompted by their importance in catalytic processes. Both experimental and theoretical studies have shown that the most thermodynamically favored product of the interaction of early and middle first-row transition-metal cations with small binary hydrides AH_n (A = C,N,O), is the H_2 elimination. This process is particularly interesting since dehydrogenation of hydrogen-containing organic and inorganic compounds is used to generate new species[37] and because of its use in industrial production (e.g., the dehydrogenation of light alkanes as an alternative method of obtaining alkenes from low-cost saturated hydrocarbon feedstock).

One of the well-known characteristics of transition metals is their ability to access to multiple low-lying electronic states and to adapt to different bonding situations, which may enable the system to find low-energy reaction paths not accessible otherwise. As a consequence, it is usually found that more than one spin surface connects reactants and products. This kind of behavior is generally referred to as two-state reactivity[36] and has been proposed to play a fundamental role in organometallic chemistry.

Several guided-ion-beam experiments[5−7,9,16,19,20] have concluded that three elimination reactions 1−3 can occur during the reaction of first-row transition metals with CH_4 and NH_3, with branching ratios varying across the series

$$M^+ + XH_n \rightarrow \begin{cases} MXH_{n-2}^+ + H_2 & (1) \\ MH^+ + XH_{n-1} \quad X=C,N & (2) \\ MXH_{n-1}^+ + H & (3) \end{cases}$$

In the case of the reaction with methane, the three observed elimination processes are endothermic for all first-row transition-metal cations. For the early and middle cations of the series, the most energetically favored process is the H_2 elimination. For the reactions with ammonia, it has been found that in the case of Sc^+, Ti^+, and V^+, the H_2 elimination is exothermic. At higher energies, the other reaction products also become accessible.

The most studied reactant has been, undoubtedly, CH_4, largely for reasons of interest in the activation of hydrocarbons. Gas-phase reaction between first-row transition-metal ions, from Sc^+ to Zn^+, with small alkanes (including methane), have been studied in a multicollisional environment.[10] Thermochemical and kinetic data for the dehydrogenation of NH_3 are only available for Sc^+, Ti^+, V^+, Co^+, Ni^+, and Cu^+.[38−41] It has been found that the minor product channels, i.e., production of MNH_2^+ and MH^+, were observed in endothermic reactions, whereas for the cases of early transition-metal cations, the formation of MNH^+ is exothermic. Bond dissociation energies (BDEs) of M^+-NH_3 complexes of first-row transition metals were determined, examining their collision-induced dissociation reactions.[42] No detailed experimental information on the mechanism and the energetics of the Mn^+ activation reactions of ammonia and methane is available in the literature. The mechanism of the

† E-mail address: nrusso@unical.it.
* Corresponding author.

10.1021/jp027344r CCC: $25.00
Published on Web 05/20/2003

reaction of manganese ion with $R-CH_3$ molecules was discussed as a result of a mass-spectrometric study in which the electronic state of the ion was varied.[14]

From the theoretical side, the properties of adducts formed upon interaction of NH_3 with first-row transition metal ions have been calculated by using a modified extended Huckel molecular orbital model[43] and their binding energies determined using the modified coupled-pair functional approach.[44] In a recent work,[35] some of us have studied the PESs of the dehydrogenation reaction of NH_3 and CH_4 molecules by Mn^+ employing DFT (B3LYP approach) and CCSD(T) levels of theory. In that work, a close description of the reaction paths leading to the three possible dissociation products has been given.

The reaction of the first-row transition-metal series with water has been studied in detail both, experimentally and theoretically.[28−31] From experimental results, it is known that early transition-metal ions (Sc^+, Ti^+, and V^+) are more reactive than their oxides, while the contrary occurs with the late metals (Cr^+, Mn^+, and Fe^+).[24] The reactivity of manganese oxide cation with dihydrogen, i.e., the inverse reaction of the one studied here, has been studied, both experimentally and theoretically, by Ryan et al.[32]

From our experience in the previously mentioned work on this subject,[35] deep difficulties arise in the interpretation of the bond information driven from traditional methods of analysis, like NBO (natural bond order). This difficulty is deeper in the case of manganese as a consequence of its particular electronic configuration. Hence, we feel that the problem must be examined with an alternative approach, to get an in-depth analysis of the reaction paths and a better understanding of the bonding transformation that takes place during the reaction. In consequence, it is not the main interest of the present work to focus on the energetic of the reactions, which has been already studied at reliable levels of theory.[31,35] The subject of this paper, instead, is to provide insight into the details of the activation processes of small ligands by transition-metal ions. To this aim, we make use of simple chemical ideas related to the bond breaking and bond formation along the reaction path, to find a topological explanation of what happens.

We present here a description of the dehydrogenation by Mn^+-(^5S,^7S) of three different isoelectronic hydrides that differs between themselves in the number of lone pairs; i.e., CH_4 (no lone pairs), NH_3 (one lone pair), and H_2O (two lone pairs). The examination of their similarities and differences from a topological point of view can give a more complete understanding of the PES (potential energy surface) behavior and on the nature of the chemical bonds occurring along them.

2. Method and Computational Details

The topological analysis of the ELF (electron localization function) gradient field provides a mathematical model enabling the partition of the molecular position space into basins of attractors, which present in principle a one to one correspondence with chemical local objects such as bonds and lone pairs. These basins are either core basins, labeled C(A), or valence basins, V(A, ...), belonging to the outermost shell and characterized by their coordination number with core basins, which is called the synaptic order. This method has been described in details elsewhere and is well documented in series of articles presenting its theoretical foundations,[45−51] its applications to the understanding of the chemical structure of molecules and solids[52−63] and the prediction of reactivity[64−66] as well as the study of chemical reactions in terms of elementary catastrophes.[67−71] Because this, we will briefly sketch the most important points of the theoretical foundations of this methodology.

The description of the electronic cloud in terms of a "chemical electron gas" has been recently introduced.[72] The chemical electron gas is characterized by two local scalar fields, the density $\rho(r)$ and the size independent spin pair composition $c_\pi(r)$:

$$c_\pi(r) = q^{-2/3}\frac{\bar{N}_V^{\alpha\alpha}(r) + \bar{N}_V^{\beta\beta}(r)}{2\bar{N}_V{}^{\alpha\beta}(r)}$$

in which $\bar{N}_V^{\alpha\alpha}(r)$, $\bar{N}_V^{\beta\beta}(r)$, and $\bar{N}_V^{\alpha\beta}(r)$ denote the integrated pair functions over a sampling volume V centered at the reference point of coordinates r whose population is q. In other words $c_\pi(r)$ is the concentration ratio of parallel and antiparallel spin pairs at a given point. It can be shown that for a closed shell single determinant wave function, $c_\pi(r)$ can be approximated within a constant by the $(D^\sigma(r)/D_0^\sigma(r))$ quantity which is the heart of the electron localization function (ELF) of Becke and Edgecombe.[45] Therefore, ELF gives a local indication of pairing directly related to the Lewis picture of the boundary.

Within the framework provided by the ELF analysis, a chemical reaction is viewed as a series of topological changes occurring along the reaction path. The parameters defining the reaction pathway, such as the nuclear coordinates and the electronic states, constitute the control space. Therefore, the topological behavior of the $D(r)$ gradient field can be studied within the framework provided by Thom's catastrophe theory.[73] This type of analysis is the so-called bonding evolution theory, whose acronym is BET.[67] There are two important indicators in using this technique, the morphic number, that is, the number of basins, and the before-mentioned synaptic order of basins.

The evolution of the bonding along the reaction path is modelled by the changes observed in the number and synaptic orders of the valence basins. Each structure is only possible for values of the control parameters belonging to definite ranges called structural stability domains. For any two points of the control space belonging to a given structural stability domain, there is the same number of critical points of each type in the ELF gradient field. This technique shows how the bonds are formed and broken and also emphasizes the importance of the geometrical constraints in a chemical reaction. Moreover, the identification of the elementary catastrophe and, therefore, the knowledge of its universal unfolding yield the dimension of the active control space governing the reaction.

From a quantitative viewpoint, the evolution of the total and spin basin populations along the path provides keys to understand the role played by the different chemical interactions. Chemical processes are then classified into three groups: the plyomorphic one, in which an increase of the morphic number is observed (e.g., a covalent bond breaking); the tautomorphic diffeosynaptic process, in which the number of basins is conserved but there is a variation of the synaptic order of at least one basin (e.g., a breaking of a dative bond); and the miomorphic process in which there is a decrease in the number of basins (e.g., covalent bond formation).

Along the reactions there exist several domains of structural stability. Within a domain of structural stability, the topology of the ELF gradient field is not altered by the variation of the control space parameters, which belong to a definite range. Between two successive domains of structural stability the evolution is ruled by a bifurcation catastrophe. At this point, at least the type of catastrophe gives access to its unfolding and, therefore, to the minimal dimension of the control space enabling

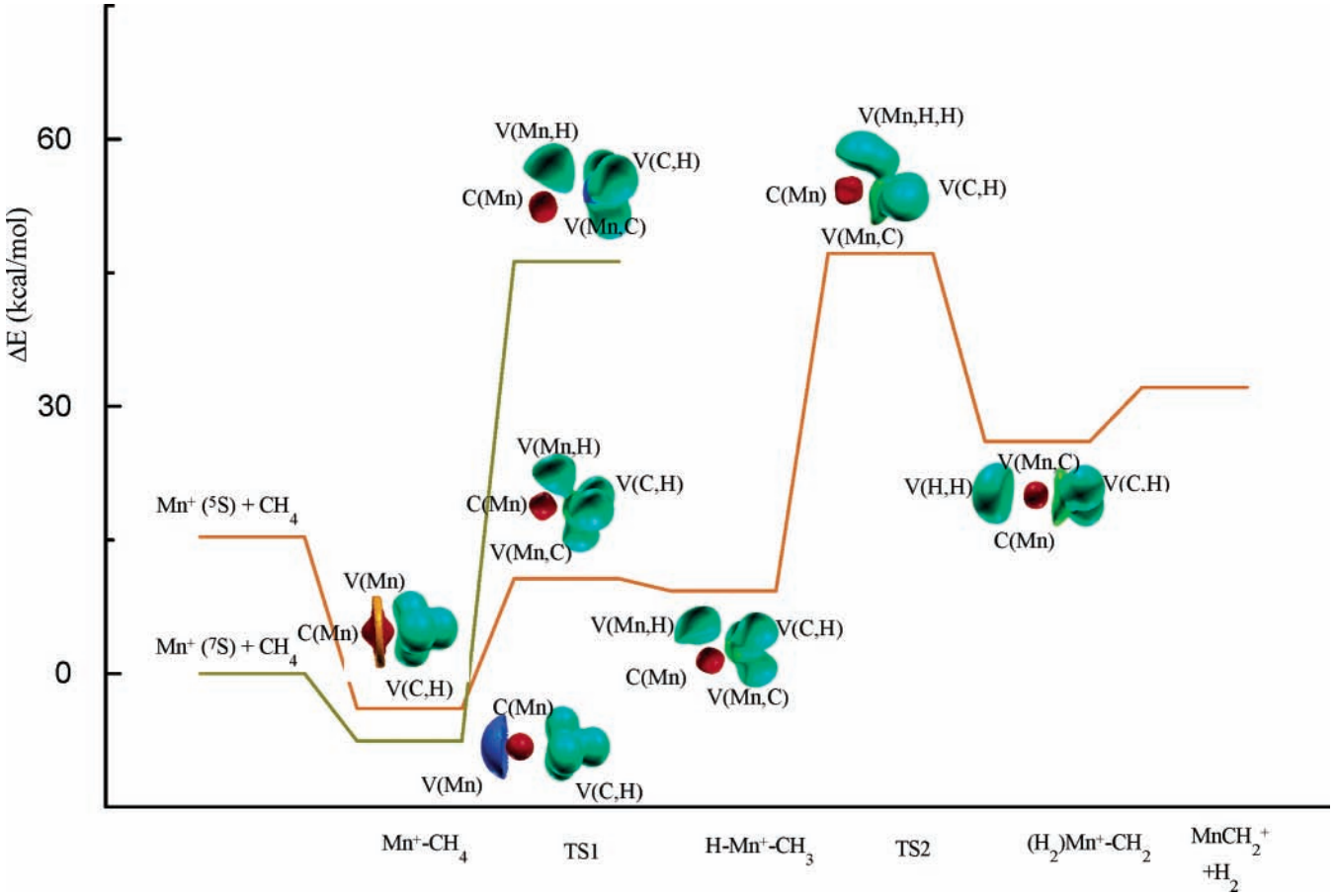

Figure 1. B3LYP/DZVP potential energy surface for the reaction of Mn^+ with CH_4 and representation of ELF localization domains for all the key minima involved in the reaction path.

the modification of the topology. Each catastrophe transforms the overall topology in such a way as the Poincaré−Hopf relation is fulfilled.

The density functional (DF) theory in its three-parameter hybrid B3LYP[74,75] formulation was the computational method used for geometry optimization and frequency calculations together with the DZVP (for the transition metal) and TZVP (for the other atoms) basis sets given by Godbout et al.[76] The choice of the B3LYP DF method was motivated by its satisfactory performance in describing transition-metal-containing systems even for complex situations such as those present in open-shell transition-metal compounds. Moreover, previous works performed on this subject[28−35] have proven that this level of theory yields realistic values in agreement to those obtained with highly correlated methods, at a significantly lower computational cost.

DFT calculations have been performed with the GAUSSIAN98 program[77] while ELF ones have been carried out with the TopMod package developed at the Laboratoire de Chimie Théorique de l'Université Pierre et Marie Curie.[78,79] Isosurfaces have been visualized with the public domain scientific visualization and animation program for high performance graphic workstations named SciAn.[80]

3. Results and Discussion

In the first part of this section, we will describe in detail the general reaction trend and the topological changes found along the PES's, trying to underline the similarities and differences among the different ligands. In the second part, we will analyze in detail the evolution of the basin populations that takes place during the reactions.

In all the studied reactions the overall energetic profiles have proved to be similar (see Figures 1−3), showing that high- and low-spin potential energy surfaces cross once in the entrance channel, just after the formation of the first ion−dipole complex. The reactions are endothermic in all cases, with endothermicity increasing from H_2O to CH_4. The full reaction profiles for the elimination reaction as well as for the minor dissociation channels are further described in refs 31 and 35.

The first step of the reaction is the formation of a stable ion-dipole complex (**I**), which is the most stable species along the reaction path. The next step, i.e., H−A (A = O, N, C) bond breaking, takes place through the Mn^+ insertion into an H−A bond, overcoming a three center transition state, to form a low-spin $H-Mn^+-AH_{n-1}$ intermediate (**II**). The reaction, then, proceeds through a concerted four-center elimination of H_2.

3.1. Bonding Evolution. 3.1.1. First Stage of the Dehydrogenation Process: From the Mn^+ Insertion into A−H Bond to the Formation of the First Reaction Intermediate, $HMnAH_{n-1}^+$. In all the studied reactions the ion−molecule complex (**I**) ground state has a septet spin state. Parts a and b of Figure 4 display the localization domain reduction tree diagrams[51] of the structures. Two different tree diagrams are observed according to the existence or not of lone pairs on the ligand central atom. For the interaction with methane (Figure 4a) the localization reduction of the valence domains first splits those related to Mn^+, namely V(Mn) and C(Mn), from the remaining valence domains. The second separation involves the V(C,H) ligand basins. In the case of the species in which lone pairs are present (Figure 4.b) the second separation involves the V(Mn,A) basins.

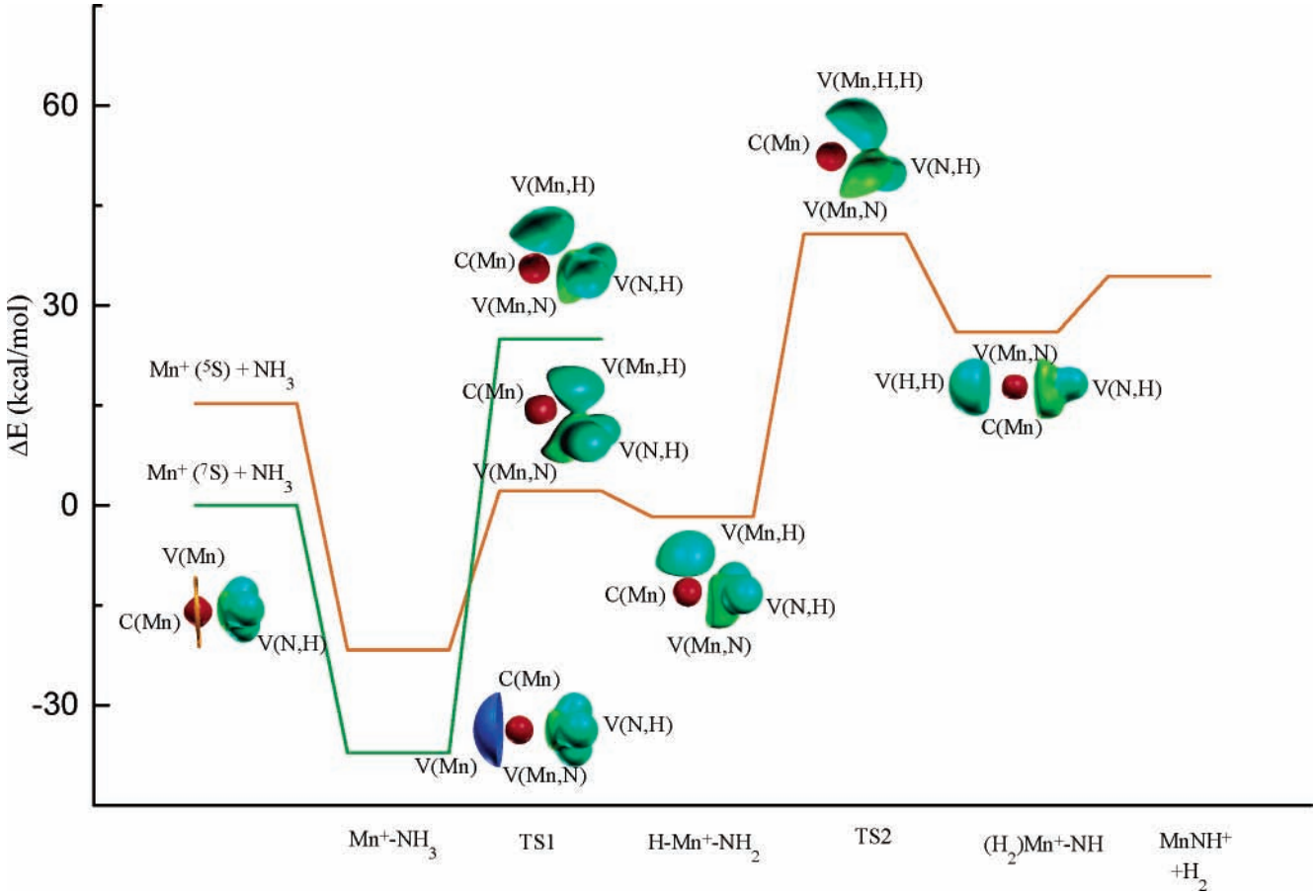

Figure 2. B3LYP/DZVP potential energy surface for the reaction of Mn^+ with NH_3 and representation of ELF localization domains for all the key minima involved in the reaction path.

As has been previously mentioned, after the formation of the first complex, an intersystem crossing between the high- and low-spin potential energies surfaces occurs, in all three studied reactions.

Figure 1 shows the localization domains corresponding to all the important minima and transition states for the reaction with CH_4. In that figure, we include the topological structures of the first minimum (**I**) and of TS1 for the two different spin states. The rest of the figures corresponds to the lowest-energy quintet spin states. It can be seen that in the case of the initial complex (**I**) the localization of the V(Mn) basin is quite different depending on its spin multiplicity. The relative locations of the V(Mn) and V(C,H) attractors in the septet spin complex makes almost impossible the charge transfer from V(Mn) to the CH_4 moiety. This fact explains the energetic difference among the first minimum and the first transition state, TS1, in the septet spin state (57.33 kcal/mol at B3LYP/TZVP level of theory; see ref 35 for details). The spin density, which is mainly located in the C(Mn) basin (see Table 1), provides another support for this description. Contrarily, in the quintet spin state V(Mn) is a torus (structurally unstable), which promotes the transference of charge from this basin toward the ligand. As a consequence of this charge transfer, the V(Mn) basin disappears and a cusp catastrophe occurs (miomorphic process). At the same time, an hyperbolic umbilic catastrophe takes place, an index 2 saddle point that lies on the separatrix of the three V(C,H) basins, is transformed into an attractor (index 0) saddle point that promotes the formation of the V(Mn,C) basin.

Continuing on the reaction path to the first transition state, TS1, another umbilic catastrophe changes the synaptic order of V(CH) basin, which becomes monosynaptic V(H), and close to TS1 V(Mn,H).

In the case of NH_3 (H_2O) the mechanism is simplified by the presence of the lone pair (the two lone pairs) which directly forms a V(Mn,N) (V(Mn,O), in the case of H_2O) basin in the complex, without a simultaneous plyomorphic process, since the miomorphic one is enough to prepare the complex in the topology of TS1.

From the TS1 to the intermediate **II** there is no topological change in the bonding since the intermediate belongs to the same structural stability domain as TS1. Figure 2 displays the localization domains corresponding to the species involved in the reaction with ammonia whereas Figure 3 shows the corresponding to the reaction with water.

3.1.2. Second Stage of the Reaction: From the Insertion Intermediate (II) to the Molecular Hydrogen Complex (III). A cusp catastrophe occurs at this point of the reaction, which involves the attractors of the V(Mn,H) and of one V(A,H) basin (A = O, N, C), together with the index 1 saddle point lying in the separatrix of the two former basins. This process can be identified as miomorphic. The resulting basin is a trisynaptic one V(Mn,H,H), which corresponds to the condensation of two covalent bonds into a three-center bond, which is expected to be dative. The further evolution of the location of the valence basins is driven mostly by the Pauli repulsion between the V(Mn,H,H) and V(Mn,A) basins. At the end, the system adopts a T-shape geometry, which is consistent with the prediction of the VSEPR[81,82] models.

3.2. Evolution of the Basins Population. The population of the core and valence basins of the $MnAH_n^+$ moieties evidence

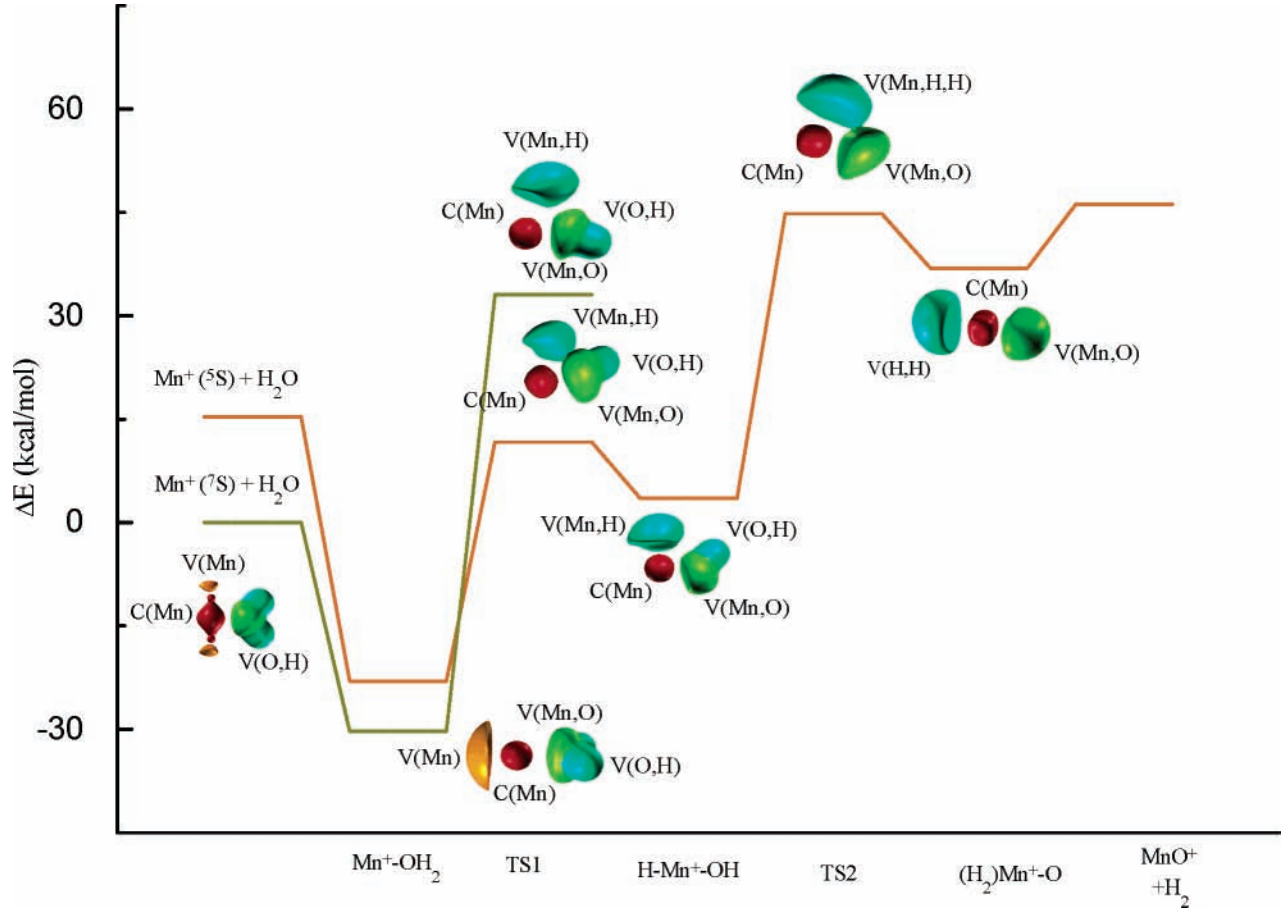

Figure 3. B3LYP/DZVP potential energy surface for the reaction of Mn^+ with H_2O and representation of ELF localization domains for all the key minima involved in the reaction path.

two different behaviors according to the presence of lone pairs in the AH_n unit. On one hand, for CH_4 the core population of Mn^+ is greater than the expectation (i.e., 23 electrons); therefore, the V(Mn) basin is populated by only 0.45 and 0.30 electrons in the septet and quintet states, respectively. Moreover, the multiplicity change induces a small electron transfer of 0.15 electrons toward the core. It is worth noting that the spin density is uniquely located in C(Mn) in the quintet state (see Table 1). On the other hand, the septet state of the NH_3 and H_2O complexes follow the expectation, moreover, the V(Mn) basin population slightly increases upon the lowering of the multiplicity as can be seen in Tables 2 and 3, respectively.

In all cases, the C(Mn) population for the TS1 is close to 23; therefore, there has been a net electron transfer of nearly one electron toward the AH_n moiety, which is now linked to a formal Mn^{2+} cation by a weak dative bond. The signature of this weak dative bond is the V(Mn,A) basin, which has a population larger than the V(A) lone pair by one electron. In the case of the water molecule, the presence of a second lone pair enables a second-order charge transfer from V(Mn, O) toward V(O). In all systems the V(Mn,H) basin population is close to 1.5.

As the complexes evolve toward the insertion intermediate (**II**), the population of V(Mn,H) basin slightly increases at the expense of the manganese core population, which is an indication of the increase of the MnH bond strength. In MO words, this means that the contribution of the 3d orbital to this bond increases. The V(A,Mn) basin population depends on the nature of the ligand and increases from 0.01 to 0.17 electrons with the number of lone pairs of atom A in the isolated ligand. This charge transfer can be roughly written as $\delta q = (4 - n) \times$

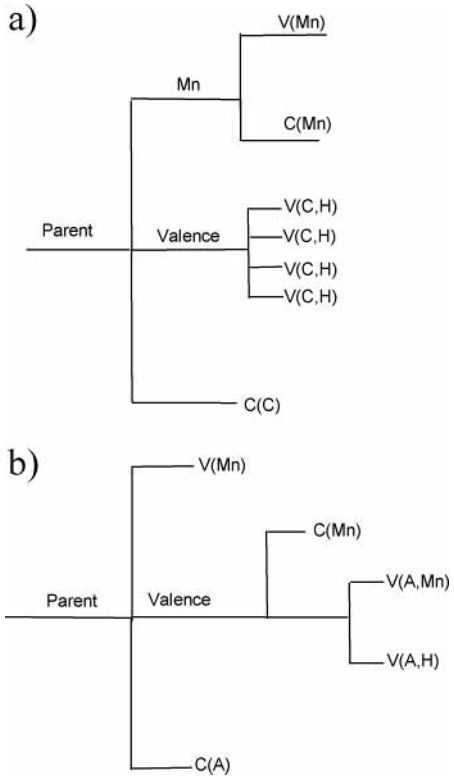

Figure 4. (a) Localization domain reduction tree diagram of $MnCH_4^+$. (b) Localization domain reduction tree diagram of $MnAH_n^+$ (A = N, O; n = 3,2).

TABLE 1: Basin Population, $\tilde{N}$, and Integrated Spin Densities, $\langle S_z \rangle$, of the Key Minima Found along of the Reaction Path of Mn^+ (^7S) and CH_4

	I ($^7A_1$)		**I** ($^5A_1$)		TS1 ($^5A'$)		**II** ($^5A'$)		TS2 ($^5A'$)		**III** ($^5A'$)		**IV** ($^5B_1$)	
basin	$\tilde{N}$	$\langle S_z \rangle$	$\tilde{N}$	$\langle S_z \rangle$	$\tilde{N}$	$\langle S_z \rangle$	$\tilde{N}$	$\langle S_z \rangle$	$\tilde{N}$	$\langle S_z \rangle$	$\tilde{N}$	$\langle S_z \rangle$	$\tilde{N}$	$\langle S_z \rangle$
C(Mn)	23.59	2.73	23.68	2.02	23.15	1.98	22.99	2.02	23.43	1.56	23.10	2.15	23.10	2.18
V(Mn)	0.45	0.21	0.30	−0.04										
C(C)	2.11	-	2.11	-	2.10		2.10	−0.01	2.10	0.01	2.10		2.10	
V(C,H)	1.96	0.01	1.98	0.01	2.05		2.08		2.09	0.06	2.08	−0.06	2.10	−0.06
V(C,Mn)					1.01		1.02		1.97	0.17	1.30	−0.02	1.25	−0.02
V(C,Mn)											1.32	−0.02	1.32	−0.02
V(H,Mn)					1.57	0.02	1.64	0.01						
V(Mn,H,H)									2.32	0.14				
V(H,H)											1.99	0.02		

TABLE 2: Basin Population, $\tilde{N}$, and Integrated Spin Densities, $\langle S_z \rangle$, of the Key Minima Found along of the Reaction Path of Mn^+ (^7S) and NH_3

	I ($^7A_1$)		**I** ($^5A_1$)		TS1 ($^5A'$)		**II** ($^5A'$)		TS2 ($^5A'$)		**III** ($^5A'$)		**IV** ($^5A_1'$)	
basin	$\tilde{N}$	$\langle S_z \rangle$	$\tilde{N}$	$\langle S_z \rangle$	$\tilde{N}$	$\langle S_z \rangle$	$\tilde{N}$	$\langle S_z \rangle$	$\tilde{N}$	$\langle S_z \rangle$	$\tilde{N}$	$\langle S_z \rangle$	$\tilde{N}$	$\langle S_z \rangle$
C(Mn)	22.98	2.43	22.81	1.95	23.08	2.02	22.89	2.00	23.10	2.11	23.13	2.11	23.17	2.20
V(Mn)	1.04	0.48	1.23											
C(N)	2.12	-	2.12		2.11		2.12		2.11	−0.01	2.11	−0.01	2.10	−0.02
V(N,H)	1.94	0.01	1.96		2.08		2.08	−0.01	2.07	−0.03	2.07	−0.05	2.07	−0.05
V(N,Mn)	2.02	0.06	1.94	0.03	3.05	−0.02	3.14		2.10	−0.01	2.41	−0.06	2.79	−0.13
V(N,Mn)									2.47	−0.06	2.26	−0.03	1.86	−0.01
V(H,Mn)					1.58	-	1.69	0.02						
V(Mn,H,H)									2.15					
V(H,H)											1.99	0.03		

TABLE 3: Basin Population, $\tilde{N}$, and Integrated Spin Densities, $\langle S_z \rangle$, of the Key Minima Found along of the Reaction Path of Mn^+ (^7S) and H_2O

	I ($^7A_1$)		**I** ($^5A_1$)		TS1 (^5A)		**II** ($^5A'$)		TS2 ($^5A'$)		**III** ($^5A'$)		**IV** ($^5\Pi$)	
basin	$\tilde{N}$	$\langle S_z \rangle$	$\tilde{N}$	$\langle S_z \rangle$	$\tilde{N}$	$\langle S_z \rangle$	$\tilde{N}$	$\langle S_z \rangle$	$\tilde{N}$	$\langle S_z \rangle$	$\tilde{N}$	$\langle S_z \rangle$	$\tilde{N}$	$\langle S_z \rangle$
C(Mn)	23.04	2.47	22.99	2.00	23.12	2.05	22.88	1.95	23.04	1.95	23.37	1.42	23.22	2.25
V(Mn)	0.98	0.45	1.08											
C(O)	2.12	-	2.14		2.13	−0.03	2.13		2.12		2.11	0.03	2.13	−0.02
V(O,H)	1.69	-	1.69		1.79		1.82	0.01						
V(O,Mn)	2.20	0.25	2.19		2.50		2.72	0.03	3.36		3.41	0.27	3.18	−0.10
V(O,Mn)	2.28	0.27	2.28		3.02		2.87	0.03	3.38		3.08	0.26	3.46	−0.12
V(H,Mn)					1.43	−0.06	1.58	−0.03						
V(Mn,H,H)									2.09	0.04				
V(H,H)											2.01	0.03		

0.085 (n = number of hydrogen atoms). In the particular case of the water molecule, as the geometry evolves toward a more symmetrical structure, another charge transfer occurs between the two V(Mn, O) basins in order to equalize their populations. The same reason can be invoked to explain the evolution of the V(Mn,N) localization domain shape, which is less distorted in **II** than in TS1.

The transition from intermediate **II** to TS2 is achieved through the increase of the V(Mn,A) population, which gains 0.95, 1.43, and 1.15 electrons for CH_4, NH_3, and H_2O, respectively. These gains are mostly due to a charge transfer from the V(Mn,H) and V(A,H) basins, which reunify into a single V(Mn,H,H) basin, whose population cannot exceed 2.5 electrons. The actual values 2.32 (CH_4), 2.15 (NH_3), and 2.09 (H_2O), are correlated with the number of lone pairs in the initial reactant. The formation of the next intermediate state (**III**) involves rather small charge transfers. On one hand, the V(Mn,H,H) population tends to two, to enable the further detachment of the H_2 molecule. On the other hand, this charge loss induces a transfer toward the V(Mn,A) basin form A = C, N. In the case of the water ligand, the V(Mn,O) population is already very high at TS2, and therefore, the electronic reorganization tends to spread the electron density yielding an increase of the C(Mn) population. Within the resonance representation, the MnO^+ entity can be understood as arising from ionic and covalent structures.

4. Conclusions

The topological analysis of the activation of three different binary hydrides by Mn^+ enables one to identify two different bonding mechanisms depending on the presence of lone pairs in the ligand. In all cases it is verified that the formation of the first ion−molecule complex in its quintet spin state promotes the charge transfer from a V(Mn) basin due to its particular spatial distribution. In the case of the reaction with methane the formation of the first intermediate of the reaction is consequence of a cusp catastrophe that causes the vanishing of the valence basin of the cation, followed by a hyperbolic umbilic catastrophe, which promotes the formation of the Mn−C valence basin. In the case of lone pair-containing molecules, the first part of the reaction is simpler due to the presence of a dative bond in the initial complex. Hence, only a miomorphic process is enough to prepare the complex in the topology of the first transition state.

After the formation of the first reaction intermediate, all the three reactions are equivalent from a bonding evolution viewpoint, since the presence of a trisynaptic basin, which corresponds to the condensation of two covalent bonds into a three-center bond, is verified in all the three cases.

Acknowledgment. Financial support from the Università degli Studi della Calabria and MIUR is gratefully acknowledged.

References and Notes

(1) Freas, R. B.; Ridge, D. P. *J. Am. Chem. Soc.* **1980**, *102*, 7129.
(2) Aristov, A.; Armentrout, P. B. *J. Am. Chem. Soc.* **1984**, *106*, 4065.
(3) Tolbert, M. A.; Beauchamp, J. L. *J. Am. Chem. Soc.* **1984**, *106*, 8117.
(4) Reents, W. L.; Strobel, F.; Freas, R. B.; Wronka, J.; Ridge, D. P. *J. Phys. Chem.* **1985**, *89*, 5666.
(5) Aristov, N.; Armentrout, P. B. *J. Phys. Chem.* **1986**, *108*, 1806.
(6) Kang, N.; Beauchamp, J. L. *J. Am. Chem. Soc.* **1986**, *108*, 7502.
(7) Aristov, N.; Armentrout, P. B. *J. Phys. Chem.* **1987**, *91*, 6178.
(8) Sunderlin, L. S.; Armentrout, P. B. *J. Phys. Chem.* **1988**, *92*, 1209.
(9) Georgiadis, R.; Armentrout, P. B. *J. Phys. Chem.* **1988**, *92*, 7067.
(10) Tonkyn, R.; Ronan, M.; Weisshaar, J. C. *J. Phys. Chem.* **1988**, *92*, 92.
(11) Buckner, S. W.; Gord, J. R.; Freiser, B. S. *J. Am. Chem. Soc.* **1988**, *110*, 6606.
(12) Irikura, K. K.; Beauchamp, J. L. *J. Am. Chem. Soc.* **1989**, *111*, 75.
(13) Sunderlin, L. S.; Armentrout, P. B. *J. Am. Chem. Soc.* **1989**, *111*, 3845.
(14) Sunderlin, L. S.; Armentrout, P. B. *J. Phys. Chem.* **1990**, *94*, 3589.
(15) Magnera, T. F.; David, D. E.; Michl, J. *J. Am. Chem. Soc.* **1989**, *111*, 4100.
(16) Armentrout, P. B.; Beauchamp, J. L. *Acc. Chem. Res.* **1989**, *22*, 315.
(17) Russel, D. H., Ed. *Gas-Phase Inorg. Chem.*; Plenum: New York, 1989; p 412.
(18) Armentrout, P. B. *Annu. Rev. Phys. Chem.* **1990**, *41*, 313.
(19) Clemmer, D. E.; Sunderlin, L. S.; Armentrout, P. B. *J. Phys. Chem.* **1990**, *94*, 208.
(20) Clemmer, D. E.; Sunderlin, L. S.; Armentrout, P. B. *J. Phys. Chem.* **1990**, *94*, 3008.
(21) Armentrout, P. B. *Science* **1991**, *41*, 175−179.
(22) Fisher, E. R.; Armentrout, P. B. *J. Am. Chem. Soc.* **1992**, *114*, 2049.
(23) Guo, B. C.; Kerns, K. P.; Castleman, A. W. *J. Phys. Chem.* **1992**, *96*, 4879.
(24) Clemmer, D. E.; Aristov, N.; Armentrout, P. B. *J. Phys. Chem.* **1993**, *97*, 544.
(25) Chen, Y.; Clemmer, D. E.; Armentrout, P. B. *J. Phys. Chem.* **1994**, *98*, 11490.
(26) Chen, Y.; Armentrout, P. B. *J. Phys. Chem.* **1995**, *99*, 10775.
(27) Haynes, C. L.; Chen, Y.; Armentrout, P. B. *J. Phys. Chem.* **1995**, *99*, 9110.
(28) Irigoras, A.; Fowler, J. E.; Ugalde, J. M. *J. Phys. Chem.* **1998**, *102*, 293.
(29) Irigoras, A.; Fowler, J. E.; Ugalde, J. M. *J. Am. Chem. Soc.* **1999**, *121*, 574.
(30) Irigoras, A.; Fowler, J. E.; Ugalde, J. M. *J. Am. Chem. Soc.* **1999**, *121*, 8549.
(31) Irigoras, A.; Elizalde, O.; Silanes, I.; Fowler, J. E.; Ugalde, J. M. *J. Am. Chem. Soc.* **2000**, *122*, 114.
(32) Ryan, M. F.; Fiedler, A.; Schroder, D.; Schwarz, H. *J. Am. Chem. Soc.* **1995**, *117*, 2033.
(33) Russo, N.; Sicilia, E. *J. Am. Chem. Soc.* **2001**, *123*, 2588.
(34) Sicilia, E.; Russo, N. *J. Am. Chem. Soc.* **2002**, *124*, 1471.
(35) Michelini, M. C.; Sicilia, E.; Russo, N. *J. Phys. Chem.* **2002**, *106*, 8937.
(36) Schroder, D.; Shaik, S.; Schwarz, H. *Acc. Chem. Res.* **2000**, *33*, 139.
(37) Chen, Z. Y.; Walder, G. J.; Castleman, A. W. *Phys. Rev. B* **1994**, *49*, 2739.
(38) Clemmer, D. E.; Sunderlin, L. S.; Armentrout, P. B. *J. Phys. Chem.* **1990**, *94*, 208.
(39) Clemmer, D. E.; Sunderlin, L. S.; Armentrout, P. B. *J. Phys. Chem.* **1990**, *94*, 3008.
(40) Clemmer, D. E.; Armentrout, P. B. *J. Am. Chem. Soc.* **1989**, *111*, 2033; *J. Phys. Chem.* **1991**, *95*, 3084.
(41) Nakao, Y.; Taketsugu, T.; Hirao, K. *J. Chem. Phys.* **1999**, *110*, 10863.
(42) Derek, W.; Armentrout, P. B. *J. Am. Chem. Soc.* **1998**, *120*, 3176.
(43) Tsipis, A. C. *J. Chem. Soc., Faraday Trans.* **1998**, *94*, 11.
(44) Langhoff, S. R.; Bauschlicher, C. W.; Partridge, H.; Sodupe, M. *J. Phys. Chem.* **1991**, *95*, 10677.
(45) Becke, A. D.; Edgecombe, K. E. *J. Chem. Phys.* **1990**, *92*, 5397.
(46) Savin, A.; Becke, A. D.; Flad, J.; Nesper, R.; Preuss, H.; von Schnering, H. G. *Angew. Chem., Int. Ed. Engl.* **1991**, *30*, 409.
(47) Savin, A.; Jespen, O.; Flad, J.; Andersen, O. K.; Preuss, H.; von Schnering, H. G. *Angew. Chem., Int. Ed. Engl.* **1992**, *31*, 187.
(48) Silvi, B.; Savin, A. *Nature* **1994**, *371*, 683.
(49) Häussermann, U.; Wengert, S.; Nesper, R. *Angew. Chem., Int. Ed. Engl.* **1994**, *33*, 2073.
(50) Savin, A.; Silvi, B.; Colonna, F. *Can. J. Chem.* **1996**, *74*, 1088.
(51) Noury, S.; Colonna, F.; Savin, A.; Silvi, B. *J. Mol. Struct.* **1998**, *450*, 59.
(52) Silvi, B.; Savin, A.; Wagner, F. R. In *Modelling of Minerals and Silicated Materials*; Silvi, B., D'Arco, P., Eds.; Topics in Molecular Organization and Engineering 15; Kluwer Academic Publishers: Dordrecht, The Netherlands, 1997; pp 179−199.
(53) Savin, A.; Nesper, R.; Wengert, S.; Fässler, T. F. *Angew. Chem., Int. Ed. Engl.* **1997**, *36*, 1809.
(54) Llusar, R.; Beltrán, A.; Andrés, J.; Noury, S.; Silvi, B. *J. Comput. Chem.* **1999**, *20*, 1517.
(55) Beltrán, A.; Andrés, J.; Noury, S.; Silvi, B. *J. Phys. Chem. A* **1999**, *103*, 3078.
(56) Fuster, F.; Silvi, B. *Theor. Chem. Acc.* **2000**, *104*, 13.
(57) Silvi, B.; Gatti, C. *J. Phys. Chem. A* **2000**, *104*, 947.
(58) Choukroun, R.; Donnadieu, B.; Zhao, J. S.; Cassoux, P.; Lepetit, C.; Silvi, B. *Organometallics* **2000**, *19*, 1901.
(59) Chesnut, D. B.; Bartolotti, L. J. *Chem. Phys.* **2000**, *253*, 1.
(60) Chesnut, D. B.; Bartolotti, L. J. *Chem. Phys.* **2000**, *257*, 171.
(61) Chesnut, D. B. *J. Phys. Chem. A* **2000**, *104*, 7635.
(62) Fressigné, C.; Maddaluno, J.; Marquez, A.; Giesner-Prettre, C. *J. Org. Chem.* **2001**, *65*, 8899.
(63) Noury, S.; Silvi, B.; Gillespie, R. G. *Inorg. Chem.* **2002**, *41*, 2164.
(64) Fuster, F.; Savin, A.; Silvi, B. *J. Phys. Chem. A.* **2000**, *104*, 852.
(65) Fuster, F.; Silvi, B. *Chem. Phys.* **2000**, *252*, 279.
(66) Fuster, F.; Savin, A.; Silvi, B. *J. Comput. Chem.* **2000**, *21*, 509.
(67) Krokidis, X.; Noury, S.; Silvi, B. *J. Phys. Chem. A.* **1997**, *101*, 7277.
(68) Krokidis, X.; Goncalves, V.; Savin, A.; Silvi, B. *J. Phys. Chem. A.* **1998**, *102*, 5065.
(69) Krokidis, X.; Silvi, B.; Alikhani, M. E. *Chem. Phys. Lett.* **1998**, *292*, 35.
(70) Krokidis, X.; Vuilleumier, R.; Borgis, D.; Silvi, B. *Mol. Phys.* **1999**, *96*, 265.
(71) Krokidis, X.; Moriarty, N. W.; Lester, W. A., Jr.; Frenklach, M. *Chem. Phys. Lett.* **1999**, *314*, 534.
(72) Silvi, B. *J. Phys. Chem. A* **2002** , in press.
(73) Thom, R. *Stabilité Structurelle et Morphogénèse*; Interdictions: Paris, 1972.
(74) Becke, A. D. *J. Chem. Phys.* **1993**, *98*, 5648.
(75) Lee, C.; Yang, W.; Parr, R. G. *Phys. Rev. B* **1988**, *37*, 785.
(76) Godbout, N.; Salahub, D. R.; Andzelm, J.; Wimmer, E. *Can. J. Chem.* **1992**, *70*, 560.
(77) Frisch, M. J.; Trucks, G. W.; Schlegel, H. B.; Gill, P. M. W.; Johnson, B. G.; Robb, M. A.; Cheesman, J. R.; Keith, T. A.; Petersson, G. A.; Montgomery, J. A.; Raghavachari, K.; Al-Laham, M. A.; Zakrzewski, V. G.; Ortiz, J. V.; Foresman, J. B.; Croslowski, J.; Stefanov, B. B.; Nanayakkara, A.; Challacombe, M.; Peng, C. Y.; Ayala, P. Y.; Chen, W.; Wong, M. W.; Andres, J. L.; Peplogle, E. S.; Gomperts, R.; Martin, R. L.; Fox, D. J.; Binkley, J. S.; Defrees, D. J.; Baker, J.; Stewart, J. P.; Head-Gordon, M.; Gonzales, C.; Pople, J. A. *Gaussian 94*, Revision A.1; Gaussian, Inc.: Pittsburgh, PA, 1995.
(78) Noury, S.; Krokidis, X.; Fuster, F.; Silvi, B. *TopMod Package*; Paris, 1997.
(79) Noury, S.; Krokidis, X.; Fuster, F.; Silvi, B. *Comput. Chem.* **1999**, *23*, 597.
(80) Pepke, E.; Muray, J.; Lyons, J. *Scian (Supercomputer Computations Res. Inst.)*; Florida State University: Tallahassee, FL, 1993.
(81) Gillespie, R. J.; Nyhdm, R. S. Q. *Rev. Chem. Soc.* **1957**, *11*, 239.
(82) Gillespie, R. J. *Molecular Geometry*; Van Nostrand Reinhold: London, 1972.